Explicit construction of chaotic attractors in Glass networks — **Source link** ↗

Roderick Edwards, Etienne Farcot, Eric Foxall

Institutions: University of Victoria

Related papers:

- Analysis of continuous-time switching networks

- Stable oscillations in mathematical models of biological control systems

- The logical analysis of continuous, non-linear biochemical control networks.

- Analysis and generic properties of gene regulatory networks with graded response functions

- Geometric properties of a class of piecewise affine biological network models.

Explicit construction of chaotic attractors in Glass networks

Roderick Edwards, Etienne Farcot, Eric Foxall

Explicit construction of chaotic attractors in Glass networks[☆]

Roderick Edwards[a], Etienne Farcot[b], Eric Foxall[a]

[a]*Department of Mathematics and Statistics, University of Victoria, P.O. Box 3060 STN CSC, Victoria, B.C. Canada V8W 3R4*
[b]*CIRAD/INRIA, Virtual Plants INRIA team, UMR AGAP, TA A-108/02, 34398 Montpellier, France*

Abstract

Chaotic dynamics have been observed in example piecewise-affine models of gene regulatory networks. Here we show how the underlying Poincaré maps can be explicitly constructed. To do this, we proceed in two steps. First, we consider a limit case, where some parameters tend to ∞, and then consider the case with finite parameters as a perturbation of the previous one. We provide a detailed example of this construction, in 3-d, with several thresholds per variable. This construction is essentially a topological horseshoe map. We show that the limit situation is conjugate to the golden mean shift, and is thus chaotic. Then, we show that chaos is preserved for large parameters, relying on the structural stability of the return map in the limit case. We also describe a method to embed systems with several thresholds into binary systems, of higher dimensions. This shows that all results found for systems having several thresholds remain valid in the binary case.

Keywords: Gene regulatory networks, Piecewise-affine systems, Chaos.

1. Introduction

Modelling of gene-regulatory networks has focussed primarily on dynamical behaviours that are fairly simple: a cascade of expression states that leads to a stable configuration, or occasionally a simple stable periodic sequence of expression states. Although more complex types of behaviour are generally not seen or not studied in research involving particular gene networks, in principle networks of even a very few genes with sufficiently rich connections can produce very complex behaviour. General model frameworks for gene regulatory networks have noted this possibility, mainly in particular examples [5, 15, 8, 9, 17]. Although it is not clear what function such complex behaviour might have in natural gene networks, its apparent absence may be a result of not looking for it. Even if it is avoided by nature, there is the possibility of synthesizing networks

---

with complex behaviour, or possibly creating complex behaviour in natural systems by appropriate control mechanisms (which might disrupt an undesirable behaviour, for example). Here, we use the framework of piecewise-linear differential equations known as Glass Networks' [10, 1, 5, 6, 7, 11, 16, 21], in which the interactions are presumed to be strongly switching, so that they depend only on whether each transcription factor is above or below some threshold, or set of thresholds.

As mentioned above, chaos has been observed in several examples taken from this class of systems, but no constructive method has been provided so far to build further examples. However, from a more general perspective, it is well known that chaotic dynamics result in many cases from the simultaneous action of expansion and contraction of phase space, in transverse stable and unstable manifolds of a homoclinic point. This hyperbolicity property has led to the definition of some standard examples, which are topologically conjugate to many chaotic dynamical systems. Probably the most famous such example is the so called *Smale horseshoe* [23], which is a planar map transforming a square into a U shaped band, whence its name. It is known to occur in dynamical systems of various dimensions, and in some sense, unimodal maps of the interval can be seen as a form of one-dimensional horseshoe.
In the case of Glass networks, it is often not difficult to explicitly compute a Poincaré return map on some threshold hyperplane. In this paper we rely on this possibility to construct an example having a return map of horseshoe type. The construction is thus of geometrical nature, and proceeds in two steps. First, a limit case where some decay terms tend to zero is considered, and then the regular situation is considered as a perturbation of this limit. The extreme case can be interpreted geometrically as a situation where return maps do not contract phase space. We thus provide some hints on how the composition of affine isometries on the threshold hyperplanes of a Glass network can be used to build a horseshoe transformation, which we hope may help constructing other examples of the same type. These indications are provided in Section 4. Before that, we provide general notation and results about Glass networks in Section 2, and about chaotic dynamics in Section 3. The example itself is presented and analysed in Section 5. In a final section it is shown that Glass networks with multiple thresholds per variable can be naturally embedded in higher dimensional systems with one threshold per variable (*binary systems*). This is related to the fact that binary Glass networks in $\mathbb{R}^3$ cannot lead to chaotic dynamics when all decay rates coincide [16]. A chaotic example has been constructed in $\mathbb{R}^3$ using distinct decay rates [15], but return maps do not take a simple form in this case. Our example is three-dimensional, and thus requires several thresholds for at least one variable. Hence the final section describes how this example can be recast in the more usual binary class.

2. Piecewise-Affine Gene Regulatory Networks

2.1. General formulation

This section contains basic definitions and notation for the piecewise affine differential equations we are dealing with in this paper [10, 5, 7, 3]. These equations can be written as:

$$\frac{dx}{dt} = \kappa(x) - \Gamma x \tag{1}$$

2

where $x = (x_1 \ldots x_n)$ represent levels of expression of n interacting genes, i.e. typically protein or mRNA concentrations. We shall abuse terms by calling the n network elements *genes*. Γ is a diagonal matrix whose diagonal entries $\Gamma_{ii} = \gamma_i$, are degradation rates of variables in the system.

Since gene transcriptional regulation is often described using a steep sigmoid law, it has been proposed to use step functions instead, in order to simplify the analysis [10]. Let us denote:

$$\begin{cases} \mathsf{s}^+(x, \theta) & = & 0 & \text{if } x < \theta, \\ \mathsf{s}^+(x, \theta) & = & 1 & \text{if } x > \theta, \end{cases}$$

This describes an effect of activation, whereas $\mathsf{s}^-(x, \theta) = 1 - \mathsf{s}^+(x, \theta)$ represents repression. We leave this function undefined at its threshold value θ; further precision will be given when needed.

The map $\kappa : \mathbb{R}_+^n \to \mathbb{R}_+^n$ in (1) is in general the composition of a multi-affine function, with step functions of the form $\mathsf{s}^\pm(x_i, \theta_i)$. For each $i \in \{1, \cdots, n\}$ let us define the finite set of thresholds at which x_i may have an effect on the system:

$$\Theta_i = \{\theta_i^0, \ldots, \theta_i^{q_i}\}. \tag{2}$$

We suppose that the thresholds are ordered (i.e. $\theta_i^j < \theta_i^{j+1}$), and the extreme values $\theta_i^0 = 0$ and $\theta_i^{q_i}$ represent the range of values taken by x_i rather than thresholds.

In each rectangular domain obtained as Cartesian products of intervals bounded by values in the threshold sets (2), the function κ is constant, and thus the dynamics is affine with a diagonal linear part. These rectangles, or *boxes*, or *regular domains* [20, 4], will be conveniently mentioned using integer vectors: a box $\mathcal{D}_a = \prod_i (\theta_i^{a_i}, \theta_i^{a_i+1})$ is well characterized by its lower-corner index $a = (a_1 \ldots a_n)$. The set of boxes is then isomorphic to

$$\mathcal{A} = \prod_{i=1}^n \{0, \cdots, q_i - 1\}, \tag{3}$$

Also, the following pairs of functions will be convenient notations: $\theta_i^\pm : \mathcal{A} \to \Theta_i$, $\theta_i^-(a) = \theta_i^{a_i-1}$ and $\theta_i^+(a) = \theta_i^{a_i}$.

It is usual to call *singular domains* [20, 4] the faces of boxes having dimension $n-1$ or lower, where some $x_i \in \Theta_i \setminus \{\theta_i^0, \theta_i^{q_i}\}$. On these domains, κ is undefined, and so is the flow. However, if the normal of the vector field has the same sign on both side of these singular hyperplanes, it is possible to extend the flow by continuity on singular domains of dimension $n-1$. Such domains are sometimes called *transparent walls*, or simply *walls* hereafter. In the remainder of this paper, we will only consider trajectories crossing transparent walls.

On any regular domain of index $a \in \mathcal{A}$, the solution of equation (1) with initial condition $x^0 \in \mathcal{D}_a$ can be computed, for each coordinate i :

$$\varphi_i(x^0, t) = x_i(t) = \phi_i(a) + e^{-\gamma_i t} \left(x_i^0 - \phi_i(a) \right), \tag{4}$$

as long as $t \in \mathbb{R}_+$ is such that $x(t) \in \mathcal{D}_a$, and with

$$\phi(a) = (\phi_1(a) \cdots \phi_n(a)) = \left(\frac{\kappa_1(a)}{\gamma_1} \ldots \frac{\kappa_n(a)}{\gamma_n} \right).$$

This point is an asymptotically stable equilibrium of the flow (4), considered independently of the network context, and will be called a *focal point* in the following. Let us make the generic assumption that no focal point lies on a singular domain:

$$\forall a \in \mathcal{A}, \quad \phi(a) \in \bigcup_{a' \in \mathcal{A}} \mathcal{D}_{a'}. \qquad \textbf{(H1)}$$

If $\phi(a) \in \mathcal{D}_a$, it is an asymptotically stable steady state of system (1). Otherwise, the trajectories reach the boundary $\partial \mathcal{D}_a$ in finite time, so that the value of κ (and thus, of ϕ) changes. At this point the direction of the flow changes, evolving towards a new focal point. Hence, the trajectories are well characterised by their successive intersections with transparent walls (extending them by continuity, as mentioned previously), a fact we will describe using a *transition map*. A graphic representation is shown in Figure 1.
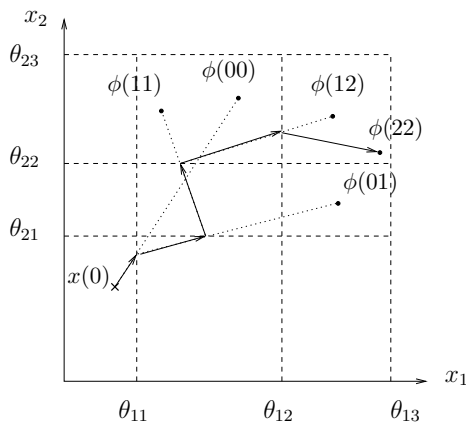

Figure 1: Schematic representation of a trajectory, with thresholds and focal points.

Let us denote $I_{out}^+(a) = \{i \in \{1, \cdots, n\} \, | \, \phi_i(a) > \theta_i^+(a)\}$, and similarly $I_{out}^-(a) = \{i \in \{1, \cdots, n\} \, | \, \phi_i(a) < \theta_i^-(a)\}$. Then, $I_{out}(a) = I_{out}^+(a) \cup I_{out}^-(a)$ is the set of escaping directions of $\mathcal{D}_a$. Now, in a given box $\mathcal{D}_a$, starting at an initial condition $x \in \mathcal{D}_a$, the time at which $x(t)$ encounters the wall $\{x \, | \, x_i = \theta_i^\pm(a)\}$, for $i \in I_{out}^\pm$, is given by

$$\tau_i(x) = \frac{-1}{\gamma_i} \ln \left(\frac{\phi_i - \theta_i^\pm}{\phi_i - x_i} \right), \qquad i \in I_{out}^\pm, \qquad (5)$$

where the index a has been omitted for simplicity. Similar omissions will be made in the sequel when there is no ambiguity. Now, $\tau(x) = \min_{i \in I_{out}} \tau_i(x)$, is the *exit time* of $\mathcal{D}_a$ for the trajectory with initial condition x. Then, we define the transition map $T^a : \partial \mathcal{D}_a \to \partial \mathcal{D}_a$:

$$\begin{aligned} T^a x &= \varphi\left(x, \tau(x)\right) \\ &= \phi + \alpha(x)(x - \phi). \end{aligned} \qquad (6)$$

where $\alpha(x) = \exp(-\tau(x)\Gamma)$. In the particular case when $\gamma_i = \gamma$, $\forall i$, Γ can be taken as scalar, and $\alpha(x)$ as well. Then, T^a is a projective transformation, and

4

many aspects of the analysis are simplified. Hence we shall consider, up to a rescaling of time, the case when

$$\forall i \in \{1, \cdots, n\},\ \gamma_i = 1. \qquad \textbf{(H2)}$$

The map above is defined locally, in a domain $\mathcal{D}_a$. However, any transparent wall can be considered as escaping in one of the two regular domains it bounds, and incoming in the other. Hence, in our context where only transparent walls are encountered, given any point of the interior of a wall, the a in expression (6) can be chosen unambiguously, and there is a well defined global transition map on the union of walls, denoted T. On the boundaries of walls, at intersections between several threshold hyperplanes, we shall extend the map T by continuity when necessary.

To conclude this section let us define the *state transition graph* $\mathsf{TG} = (\mathcal{A}, \mathcal{E})$ associated with a system of the form (1): nodes $\mathcal{A}$ represent boxes as in (3) and $(a, b) \in \mathcal{E} \subset \mathcal{A}^2$ if and only if $b = a \pm \mathrm{e}_i$, with $i \in I_{out}^{\pm}(a)$ and e_i a standard basis vector. It is not difficult to see that this is equivalent to $\partial \mathcal{D}_a \cap \partial \mathcal{D}_b \neq \varnothing$, and the existence of an open set of trajectories going from $\mathcal{D}_a$ to $\mathcal{D}_b$.

In the following, unless specified otherwise, we will consider that **(H1)** and **(H2)** hold.

3. Horseshoes and chaos

In this section we recall those of the standard definitions and results about chaotic dynamics that we will use to study our example. This essentially consists of the notion of topological entropy, some basic results about symbolic dynamics, and a rapid application of these notions to the *tent map* example. A more comprehensive introduction can be found in many textbooks in dynamical systems, e.g. [12, 22]. Since the example will rely on is a map, only discrete time dynamics are mentioned in the present section.

A topological dynamical system (X, f) is the action of a continuous map f on a compact metric space X, with metric $d(\cdot, \cdot)$, by repeated composition. Given initial condition $x \in X$, its *orbit* is defined as $\mathcal{O}(x) = \{f^n(x) \mid n \in \mathbb{N}\}$. Asymptotically, the orbits will usually accumulate in a closed subset of X, called an attractor. In simple situations, an attractor may be a periodic orbit of the form $\{x, f(x), f^2(x), ..., f^n(x) = x\}$ (a fixed point being the special case $n = 1$). But it may also have a much more complicated structure, in which case the adjective *chaotic* is often used. Several criteria have been proposed to decide whether a given, non-periodic attractor, deserves this epithet. We will not enter into a thorough discussion about these different definitions, but rely on the convenient notion of *topological entropy*. Informally, this quantity measures the exponential growth rate of the number of distinguishable orbits, when their length increases. We denote it by $h(f)$. When the entropy $h(f)$ is positive, the number of distinguishable trajectories increases exponentially with time, indicating a high level of complexity. Moreover, it is known that positive topological entropy implies sensitive dependence on initial conditions, one feature that is required by all definitions of chaos used. Among those definitions, positive topological entropy
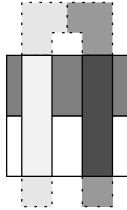
Figure 2: A square S and its image by a horseshoe transformation, f. The white and gray rectangles represent a partition leading to the full shift on $\{0, 1\}$ as symbolic dynamical system. Shaded parts, as well as all points which eventually escape the square, are not considered in the dynamics: $X = \cap_{n \leq 0} f^n(S)$.

is often used, and this will be our criterion in the following.

Let us now briefly describe two examples of chaotic systems, in the sense above.

In short, a horseshoe is a dynamical system where X is a square, and f maps X to a U shaped band in the plane by "stretching and folding", see Figure 2. Using the partition shown in the figure, it is known that this system is conjugate to the full shift on two symbols, hence its topological entropy is $\log(2)$, and it is chaotic. This complexity is topological in nature, and many deformed versions of Figure 2 have essentially the same dynamics, see e.g. [22].

Another of the best-understood examples of dynamical systems is that of unimodal maps, i.e. functions of an interval having a single maximum, and which are increasing (resp. decreasing) below (resp. above) that maximum. Such functions can intuitively be seen as one dimensional versions of a horseshoe. When considering a one-parameter family of such maps, it is known that some universal features are encountered, including a very structured cascade of bifurcations, leading to chaos via a series of period doubling events [2]. The particular example of unimodal maps of the interval we will encounter in our example are so called tent maps. Because they are not smooth, they do not exactly follow the cascade just mentioned, but a sharper one, where chaos occurs immediately after the 'period two' bifurcation. More precisely, let us define a one parameter family of maps of the interval $I = [-1, 1]$ as follows:

$$T_\mu(y) = \mu(1 - 2|y|), \qquad \text{where} \quad \mu \in (0, 1]. \qquad (7)$$

When $\mu = 1$, one shall refer to the *full* tent map. For this map, a symbolic dynamical system can be built using the partition $\{[-1, 0), (0, 1]\}$. Then, the full tent map is conjugate to the full shift on two symbols, and thus it has topological entropy $\log(2)$. More generally, if a piecewise monotone map of the interval has a derivative whose absolute value lies in $[r_1, r_2]$ at all points (for some positive constants r_1, r_2), then its entropy belongs to $[\log(r_1), \log(r_2)]$, see [18] and references therein. Hence the tent maps in (7) have entropy

$$h(T_\mu) = \log(2\mu).$$

In Figure 3, a bifurcation diagram and some typical orbits are shown.
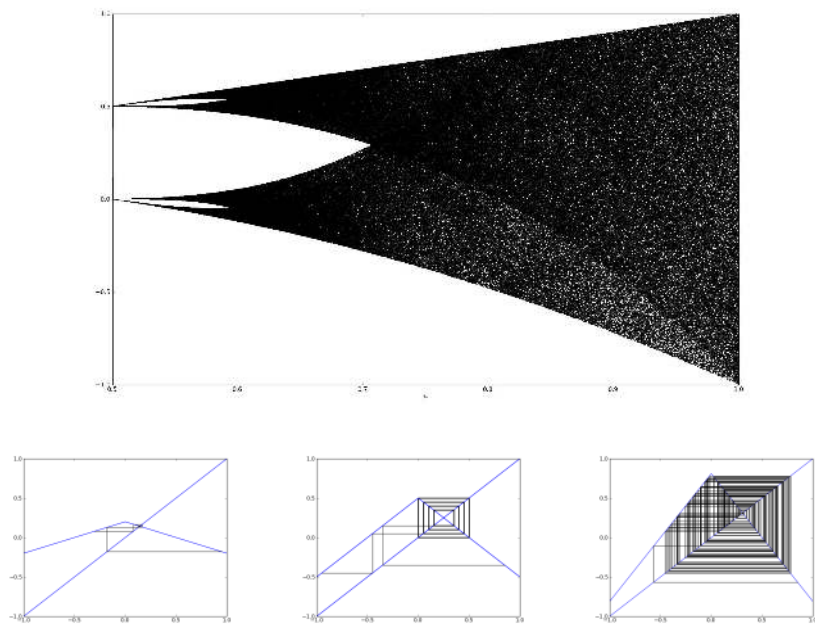
Figure 3: Bifurcation diagram for the tent maps in Equation (7), with $\mu \in [\frac{1}{2}, 1]$. Cobweb diagrams are also shown: from left to right, $\mu = \frac{1}{4}$, $\mu = \frac{1}{2}$ and $\mu = 0.810$. In the first case, as for any $\mu < \frac{1}{2}$, there is a unique stable fixed point. At $\mu = \frac{1}{2}$, all orbits are periodic with period 2, hence $h(T_{\frac{1}{2}}) = 0$. For any $\mu > \frac{1}{2}$, the entropy is positive.

4. Sequences of transitions as rotations and reflections

In this section, we return to Glass networks and consider a situation where focal points can be infinitely remote. From Eq. (5) and (6), it can be seen that in such a case the transitions occur instantaneously, and the maps do not contract walls, since $|\alpha(x)| = 1$. This claim will be considered more thoroughly in section 5. In $\mathbb{R}^3$, it follows that the transition maps act as isometries of the plane. In this section we investigate the type of isometries that may occur in this limit, and how they compose. To this aim, let us introduce two basic isometries of the plane:

$$h(x, y) = (-y, x) \qquad \text{is the rotation of angle } \tfrac{\pi}{2}, \text{ and}$$

$$g(x, y) = (x, -y) \qquad \text{is the reflexion through the first axis.}$$

From any path in the state transition diagram, a sequence of transitions can be deduced. For instance, from the path below
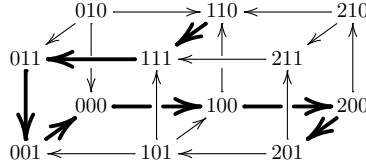
we deduce

$$3^+1^-2^-3^-1^+1^+3^+ \ldots \tag{8}$$

where the numbers represent the variables crossing a threshold at each step, and the signs indicate whether this variable is increasing or decreasing. The path above corresponds to a trajectory in phase space schematized here:
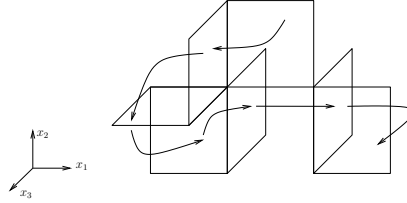
In order to deal with transformations in $\mathbb{R}^2$ only, we define a projection ρ, from the set of threshold planes in phase space to $\mathbb{R}^2$, see Figure 4.

A single transition between successive walls, say W, W', corresponds to a pair $a^i b^j$ in sequences of the form (8), for $a, b \in \{1, 2, 3\}$ and $i, j \in \{-, +\}$. This also defines a map $W \to W'$. Each wall $W \subset \{x_k = \theta_{kl}\}$ for some k and l. Under the effect of ρ, this corresponds to a map $T : \mathbb{R}^2 \to \mathbb{R}^2$.

$$
\begin{array}{ccc}
W & \xrightarrow{\ a^i b^j\ } & W' \\
\rho \downarrow & & \downarrow \rho \\
\mathbb{R}^2 & \xrightarrow{\ T\ } & \mathbb{R}^2
\end{array}
$$

A more explicit description of ρ can be given:

$$(z_1, z_2) = \begin{cases} \rho(x_1, x_2, \theta_{3l}) &=& (x_1, x_2) \\ \rho(\theta_{1l}, x_2, x_3) &=& (x_2, x_3) \\ \rho(x_1, \theta_{2l}, x_3) &=& (x_3, x_1) \end{cases}$$
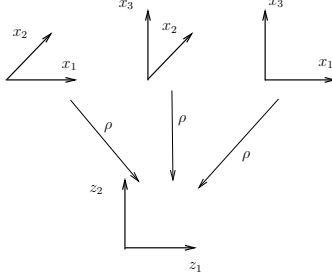
Figure 4: Projections from wall coordinates to $\mathbb{R}^2$.

Since T in the commutative diagram above may only take a finite number of values, it is possible to transcribe sequences of the form $a^i b^j$ into these transformations. Namely, we have from an exhaustive inspection:

$$\begin{cases} a^{\pm} b^{\pm} & \rightarrow & h^{-1} \\ b^{\pm} a^{\pm} & \rightarrow & h \\ a^{\pm} b^{\mp} & \rightarrow & h \circ g \\ b^{\pm} a^{\mp} & \rightarrow & h \circ g \\ a^{\pm} a^{\pm} & \rightarrow & \mathbf{1} \end{cases} \qquad \text{where } b = a + 1 \pmod 3 \qquad (9)$$

where $\mathbf{1}$ is the identity transformation. Note that transitions $a^{\pm} a^{\mp}$ cannot occur because all walls are supposed transparent.

For longer sequences like (8), the corresponding transformation in $\mathbb{R}^2$ can be obtained by composition of the elementary transformations T. The full set of rotations and reflections of the plane consists of only eight elements :

$$\{\mathbf{1}, h, h^{-1}, h^2, g, h \circ g, h^{-1} \circ g, h^2 \circ g\} \qquad (10)$$

It is easy to verify that sequences can be reduced to one of the elements of (10) by use of the following three rules:

$$\begin{aligned} h \circ g & = & g \circ h^{-1} \\ h^4 & = & \mathbf{1} \\ g^2 & = & \mathbf{1} \end{aligned} \qquad (11)$$

A schematic picture of the first rule can take this form:
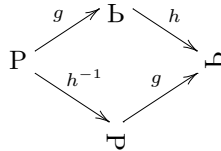
A convenient rule can also be easily deduced from the three above:

$$g \circ h^n = h^{-n} \circ g \qquad (12)$$

for any integer n.

Let us provide an example of this type of reduction, on the sequence (8). Note that the order of symbols in a sequence is written left to right, but because the transformations in $\mathbb{R}^2$ are compositions of maps, we write them from right to left.

$$3^+1^-2^-3^-1^+1^+3^+\ldots$$

becomes

$$(h)(\mathbf{1})(hg)(h^{-1})(h^{-1})(hg) = h^2gh^{-1}g = h^3g^2 = h^{-1}$$

where we omit the ∘'s for brevity. Thus, according to our definitions, this trajectory generates a clockwise rotation in the plane.

One result about cycles can be deduced from the discussion above:

Proposition 1. *If S is a sequence of transitions between walls that corresponds to a cycle in the states transition diagram, then the corresponding transformation, in reduced form, contains no reflection g.*

Proof. From the rules in (9), it is clear that g occurs exactly when a change of sign occurs in the transition sequence. In the case of a cyclic sequence, after traversing the cycle once, we must end with a transition in the same direction as the first transition. Therefore, the number of sign changes is even, and the composition of transformations of $\mathbb{R}^2$ contains an even number of g's. By repeated application of the rule (12), we can reduce the resulting transformation to the form $h^m g^{2n}$, where m and n are integers, and $g^{2n} = \mathbf{1}$. □

This proposition will help us in constructing a Horseshoe map. Actually, such a map classically involves a reflection or a rotation by π of one half of its domain, depending on the choice of axes. In our case, this will not be possible via the reflection g, hence we may restrict ourselves to looking for a map involving reflection through the other axis, that is h^2.

5. Horseshoe construction

5.1. Transition Graph

In this section we consider the map associated with the following graph, which we obtained by relying on the observations from the previous section, notably Proposition 1:

$$(13)$$
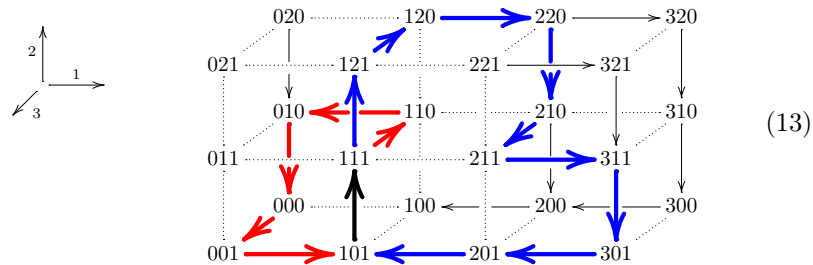
There are two cycles starting from the boundary between boxes 101 and 111:

$$111 \to 110 \to 010 \to 000 \to 001 \to 101 \to$$

and

$$111 \to 121 \to 120 \to 220 \to 210 \to 211 \to 311 \to 301 \to 201 \to 101 \to \quad .$$

Note that if these two cycles contain an invariant region for the dynamics, the focal points can be chosen arbitrarily in the remainder of the graph. The choice pictured above (e.g. with $\phi(320) \in \mathcal{D}_{310}$) corresponds to the simplest equations of the form (1) ensuring that all boxes in the two cycles have successors adapted to our construction. These equations are given in section 6, the analysis provided here relying only on transition maps, which can be computed directly from the focal point coordinates.

With the notation of the previous section, the two cycles correspond to transformations:

$$3^- 1^- 2^- 3^+ 1^+ 2^+ 3^- \longmapsto (hg)(h^{-1})(h^{-1})(hg)(h^{-1})(h^{-1}) = \mathbf{1}$$
$$2^+ 2^+ 3^- 1^+ 2^- 3^+ 1^+ 2^- 1^- 1^- 2^+ \longmapsto (hg)(\mathbf{1})(h)(hg)(h^{-1})(hg)^4(\mathbf{1}) = h^2 \quad (14)$$

5.2. Focal Points

Now, we will describe the position of focal points in the cycles. It will follow that the transition maps indeed correspond to rotations and reflections of the plane, in the limit of infinitely remote focal points.

To describe the focal point coordinates, we will use two parameters, denoted b and c, taking positive values, and such that the limit $b, c \to +\infty$ corresponds to infinitely remote focal points. The position of focal points will be similar for most boxes, up to some symmetry, and described using c. The only exceptions are boxes 201, and the three boxes $101, 111, 121$, at which the "splitting" between the two cycles occurs.

As seen on the transition graph, the focal point $\phi(201)$ has a first coordinate lower than θ_1^2, and its two other coordinates in (θ_2^0, θ_2^1) and (θ_3^1, θ_3^2), respectively. Hence we chose:

$$\phi(201) = \left(\theta_1^2 - c, \; \frac{\theta_2^0 + \theta_2^1}{2}, \; \frac{\theta_3^1 + \theta_3^2}{2} \right)$$

It is not difficult to see that in the limit $c \to \infty$, the box is mapped onto the wall $\{x_1 = \theta_1^2\}$ by the transition map, and in particular that this map acts as a translation on the parallel wall $\{x_1 = \theta_1^3\}$.

The three boxes 101, 111 and 121 will be described later. Let us now describe generically the case of all other boxes. All of them have two escaping directions, one of which corresponds to trajectories following the union of the 2 cycles. Let us denote s the latter switching direction, and r the other escaping direction, while i is the third direction, i.e. $I_{out} = \{s, r\}$ and $\{i\} = \{1, 2, 3\} \setminus \{s, r\}$; see Figure 5 for a generic representation of these boxes. For example at box 120, we have $s = 1$, $r = 3$ and $i = 2$, and indeed, some point in this box can reach the switching wall $x_r = x_3 = 2$. However, for the choice of focal points represented in Figure 5, this never holds for points that come from the preceding box 121, i.e. for the wall $x_3 = 1$. More generally, the reader may verify that at all the concerned boxes, trajectories following the cycles will always enter the box in the r direction, see Figure 5. Accordingly, the focal point will be chosen on the plane separating trajectories escaping in the r and s directions, which ensures invariance of the cycles.

For sake of generality, let us introduce another notation: for any escaping direction, $\pm_i$ is the sign such that $i \in I_{out}^{\pm_i}$, $\mp_i$ its opposite. Then, the focal
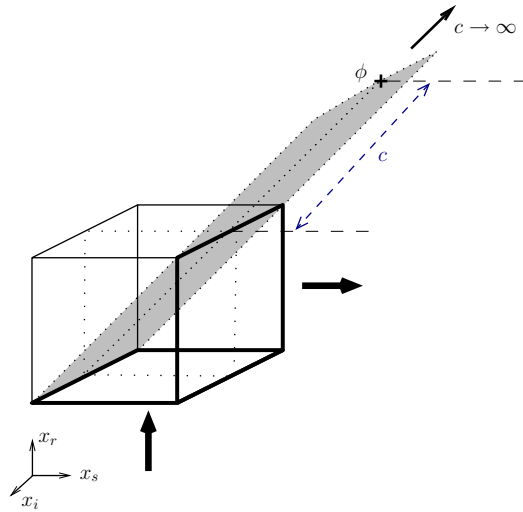
Figure 5: Typical position of the focal point in all boxes but 101, 111 and 201. Large arrows represent the path followed by trajectories in the cycles.

points coordinates can be written

$$
\begin{cases}
\phi_s &= \theta_s^{\pm_s} \pm_s c \\
\phi_r &= \theta_r^{\pm_r} \pm_r \left(\dfrac{\theta_r^+ - \theta_r^-}{\theta_s^+ - \theta_s^-} \right) c \\
\phi_i &= \dfrac{\theta_i^- + \theta_i^+}{2}
\end{cases}
$$

To simplify the expressions, we will assume from now on that threshold values are successive integers, so that in particular

$$
\theta_i^j = j \quad \text{and} \quad \theta_i^{\pm_i} - \theta_i^{\mp_i} = \pm_i 1 \qquad \forall i,
$$

and the focal point expression simplifies to:

$$
(\phi_s, \phi_r, \phi_i) = \left(\theta_s^{\pm_s} \pm_s c, \quad \theta_r^{\pm_r} \pm_r c, \quad \frac{\theta_i^- + \theta_i^+}{2} \right) \tag{15}
$$

Remark. *It appears that the two cycles are not entirely invariant, since for instance some trajectories can escape the box 220 towards 320, here ending necessarily in 100 which contains a fixed point. However, it is possible to show that all trajectories starting in box 111 remain in the union of cycles forever when focal points are of the form (15).*

Let us now consider the three boxes 101, 111 and 121 which will contain the wall we chose as a Poincaré section. To get some intuition, a schematic view of the action of the map at these boxes is shown in Figure 6. From the transition graph (13) it appears that $I_{out}(101) = \{2\}$, so that 111 is its only successor, and $I_{out}(111) = \{2,3\}$. Also, we assume $I_{out}(121) = \{2,3\}$, with all trajectories coming from 111 switching in direction 2, similarly to the other boxes discussed
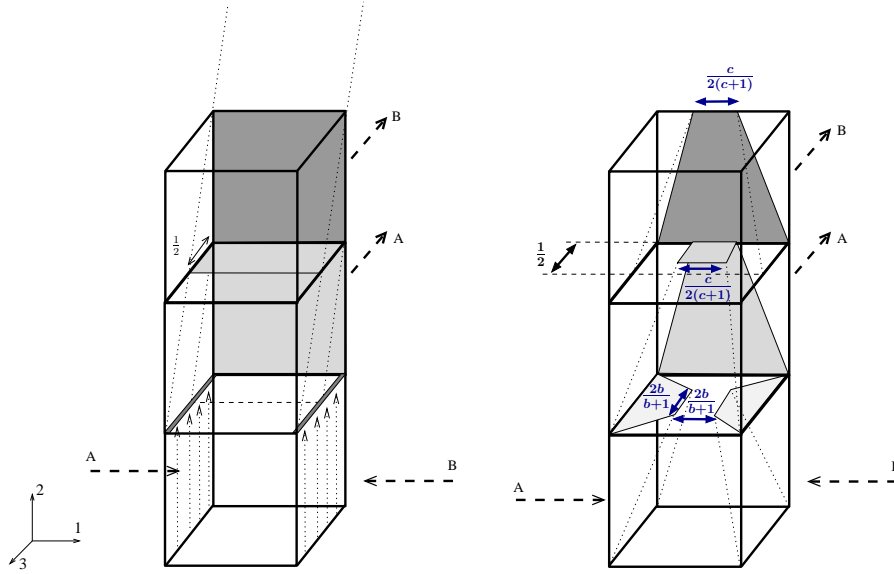
Figure 6: The three boxes 101, 111 and 121, from bottom to top, for infinite (left) and finite (right) parameters b, c. Note that in the first case, box 101 is entirely mapped onto its upper wall $\{x_2 = 1\}$. Thus the incoming walls are mapped to its left and right upper edges, as represented using grey edges and dotted arrows. Grey regions are wall images, dotted lines link some chosen points to their image. Arrows with A and B represent the shorter and longer cycles in (13), respectively. For finite b and c, some indicative lengths are shown.

above. The focal points of these boxes are given by:

$$\phi(101) = \left(\frac{3}{2},\ 1+b,\ \frac{3}{2}\right)$$

$$\phi(111) = \left(\frac{3}{2},\ 2+c,\ 1-\frac{c}{2}\right)$$

$$\phi(121) = \left(\frac{3}{2},\ 3+c,\ 1-\frac{c}{2}\right)$$

where the parameter c is the same as for other focal points, whereas b plays a similar role but is allowed to take different values in general, in order to get a specific control on the contraction occurring in box 101.

5.3. Transition Maps

Let us now express an arbitrary transition map in terms of the parameters b and c, and compute its pointwise limit when $c \to \infty$. Note that since we work under hypothesis **(H2)**, $\alpha(x)$ in (6) is scalar a take the simple form:

$$\alpha(x) = \frac{\phi_s - \theta_s^{\pm_s}}{\phi_s - x_s} Id,$$

where s is the escaping direction for x, i.e. the direction which minimizes the escaping time, equation (5). We shall omit the identity matrix Id for simplicity

13

in the following, and simply consider α as a real function.

Now, we can inject the expression (15) in the transition map expression (6). At a point x following the cycles, and thus escaping in the s direction, one gets:

$$
\begin{cases}
T_s x & = & \theta_s^{\pm_s} \\[2mm]
T_r x & = & \theta_r^{\pm_r} \pm_r c + \dfrac{\pm_s c}{\theta_s^{\pm_s} \pm_s c - x_s}\left(x_r - \theta_r^{\pm_r} \mp_r c\right) \\[4mm]
T_i x & = & \dfrac{\theta_i^+ + \theta_i^-}{2} + \dfrac{\pm_s c}{\theta_s^{\pm_s} \pm_s c - x_s}\left(x_i - \dfrac{\theta_i^+ + \theta_i^-}{2}\right)
\end{cases}
\tag{16}
$$

For our choice of the threshold values and focal points, see (15) and the definition of directions (s, r, i), we have that $x_r = \theta_r^{\mp_r}$ for any point whose orbits follows one or the two cycles. Hence, we can in fact write:

$$
T_r x = \theta_r^{\pm_r} + \dfrac{\pm_r c\,[\theta_s^{\mp_s} - x_s]}{\theta_s^{\pm_s} \pm_s c - x_s}
$$

and in the limit $c \to \infty$, the following expressions are easily obtained:

$$
\begin{cases}
T_r^\infty x & = & \theta_r^{\pm_r} + \pm_s \pm_r \left(\theta_s^{\mp_s} - x_s\right) \\[4mm]
T_i^\infty x & = & x_i
\end{cases}
$$

In other words, up to a translation sending the thresholds $\theta_r^{\pm_r}$ and $\theta_s^{\mp_s}$ to zero, the limit map T^∞ acts on the walls as the identity, or a reflection (depending on the signs $\pm_r$ and $\pm_s$). Notice also that ignoring the coordinates that equal a threshold, both on the domain and range of a the transition map above, the remaining coordinates are (x_s, x_i) and (x_r, x_i) respectively. Defining a planar map using the projection $\rho : \mathbb{R}^3 \to \mathbb{R}^2$ defined in section 4, it may happen that (x_s, x_i) is in fact mapped to (x_i, x_r), i.e. there is a $\pm\frac{\pi}{2}$ rotation (this happens for instance for $(s, r) = (1, 2)$ as occurs e.g. at boxes 010 or 220). In all cases, it is clear that it $\rho \circ T^\infty$ is either a rotation, a reflection, or the identity, as expected.

Now we have all the information to compute the transition maps of the three remaining boxes $101, 111$ and 121. First 101 and 121, respectively:

$x = (\theta_1^\pm, x_2, x_3),$

$$
T(x) = \begin{bmatrix} \frac{3}{2} + \frac{b}{b+1-x_2}(\theta_1^\pm - \frac{3}{2}) \\[2mm] 1 \\[2mm] \frac{3}{2} + \frac{b}{b+1-x_2}(x_3 - \frac{3}{2}) \end{bmatrix}
$$

$x = (x_1, 2, x_3),$

$$
T(x) = \begin{bmatrix} \frac{3}{2} + \frac{c}{2x_3+c-2}(x_1 - \frac{3}{2}) \\[2mm] c + 3 - \frac{c}{2x_3+c-2}(c+1) \\[2mm] 1 \end{bmatrix}
$$

where $\theta_1^\pm \in 1, 2$ for the first map, depending on the incoming wall. At box 111, the two escaping walls can be reached, and the transition map reads:

$x = (x_1, 1, x_3),$

$$
\begin{bmatrix} \frac{3}{2} - \alpha(x)(\frac{3}{2} - x_1) \\[2mm] c + 2 - \alpha(x)(c+1) \\[2mm] 1 - \frac{c}{2} - \alpha(x)(1 - \frac{c}{2} - x_3) \end{bmatrix}
\quad \text{where } \alpha(x) = \begin{cases} \dfrac{c}{c + 2x_3 - 2} & \text{if} \quad x_3 < \frac{3}{2} \\[4mm] \dfrac{c}{c+1} & \text{if} \quad x_3 > \frac{3}{2} \end{cases}
$$

Let us consider the limit maps obtained as $c \to \infty$, again denoted T^∞:

- At box 101, if $b \to \infty$ as well: $T_1^\infty x = \theta_1^\pm$ $T_2^\infty x = 1$ $T_3^\infty x = x_3$.
  Hence the incoming walls are sent to the edges $\{x_1 = \theta_1^\pm,\ x_2 = 1\}$, as seen on figure 6.

- At box 111:
  $$T_1^\infty x = x_1 \qquad T_2^\infty x = 2x_3 - 1 \qquad T_3^\infty x = 1 \quad \text{for } x_3 < \tfrac{3}{2}, \quad \text{and}$$
  $$T_1^\infty x = x_1 \qquad T_2^\infty x = 2 \qquad T_3^\infty x = x_3 - \tfrac{1}{2} \quad \text{for } x_3 > \tfrac{3}{2}.$$

- At box 121: $T_1^\infty x = x_1 \qquad T_2^\infty x = 2x_3 \qquad T_3^\infty x = 1$.

Since we have seen that at all other boxes, T^∞ acts as a rotation, a reflection or a translation, it is mostly a matter of tracking index switchings to obtain an explicit expression for the Poincaré return map on the wall $W = [1,2] \times \{1\} \times [1,2] = \overline{\mathcal{D}}_{101} \cap \overline{\mathcal{D}}_{111}$. Depending on $x_3 > \tfrac{3}{2}$ or the reverse, the map crosses one cycle or the other. In fact, $(x_1, 1, x_3) \in W$ follows the sequence of isometries below:

- if $x_1 < \tfrac{3}{2}$: $(x_1, 1, x_3) \to (x_1, 2x_3 - 1, 1) \to (1, 2x_3 - 1, 2 - x_1) \to (3 - 2x_3, 1, 2 - x_1) \to (3 - 2x_3, 2 - x_1, 1) \to (1, 2 - x_1, 2x_3 - 1) \in \{1\} \times [1,2]^2$.

- if $x_1 > \tfrac{3}{2}$: $(x_1, 1, x_3) \to (x_1, 2, x_3 - \tfrac{1}{2}) \to (x_1, 2x_3 - 1, 1) \to (2, 2x_3 - 1, x_1 - 1) \to (2x_3 - 1, 2, x_1 - 1) \to (2x_3 - 1, x_1, 1) \to (3, x_1, 5_2 x_3) \to (2 + x_1, 1, 5 - 2x_3) \to (3, 2 - x_1, 5 - 2x_3) \to (2, 2 - x_1, 5 - 2x_3) \in \{2\} \times [1,2]^2$.

Then, applying the local map of D_{101} to $(1, 2 - x_1, 2x_3 - 1)$ and $(2, 2 - x_1, 5 - 2x_3)$, and ignoring the second coordinate since it is fixed to 1, provides us with the following return map:

$$P(x_1, x_3) = \begin{cases} \left(\dfrac{3(x_1 - 1) + 2b}{2(b + x_1 - 1)},\ \dfrac{3(x_1 - 1) - 2b + 4bx_3}{2(b + x_1 - 1)} \right) & \text{if} \quad x_1 < \tfrac{3}{2}, \\[3mm] \left(\dfrac{3(x_1 - 1) + 4b}{2(b + x_1 - 1)},\ \dfrac{3(x_1 - 1) + 10b - 4bx_3}{2(b + x_1 - 1)} \right) & \text{if} \quad x_1 > \tfrac{3}{2}. \end{cases}$$
$$\tag{17}$$

We now develop some analysis of this return map.

5.3.1. Study of the return map in the limit $c \to \infty$

It will be much more convenient to rescale this planar map, so that it acts on the square $D = I^2$, where $I = [-1, 1]$, with zero as a threshold instead of $\tfrac{3}{2}$. Indeed, the map above then takes the simpler form:

$$F(x, y) = \frac{2b}{x + 2b + 1} \big(\mathrm{sgn}(y), 1 - 2|y| \big), \tag{18}$$

where the scalar function $\mu(x) = \mu(x; b) = \frac{2b}{x + 2b + 1}$ acts multiplicatively on both coordinates. We will denote F_1 and F_2 the two coordinate functions of F in the following.

Although the expression (18) is formally defined for $y = 0$, the horizontal line $I \times \{0\}$ is in fact a discontinuity line for F, since the restrictions on $y < 0$ and $y > 0$ take different values in the limit $y \to 0$:

$$F^-(x, 0) \doteq \lim_{\substack{y \to 0 \\ y < 0}} F(x, y) = (-\mu(x), \mu(x)),$$

and

$$F^+(x,0) \doteq \lim_{\substack{y \to 0 \\ y > 0}} F(x,y) = (\mu(x), \mu(x)).$$

More generally, we will respectively denote F^- and F^+ the restrictions of F to the rectangles $I \times [-1,0]$ and $I \times [0,1]$, using the two previous limits on $I \times \{0\}$. Two avoid repeated discussions on the discontinuity line, and to deal with compact sets only, we will first consider that the map F is two-valued on this line, taking both F^- and F^+ values. Only at the end of the section, we will return to this question and discuss the consequences of this extension.
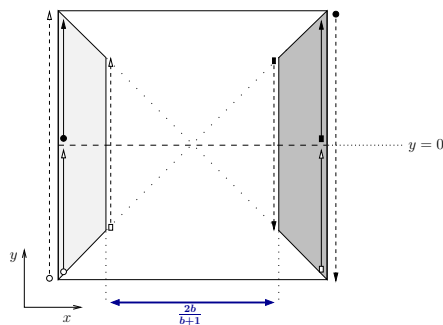

Figure 7: Schematic view of the return map (18) in the case $b < \infty$, $c \to \infty$. The light and dark gray regions are respectively the images of the $y < 0$ and $y > 0$ halves of the square. The slanted boundaries of these regions are aligned with the origin, as indicated by dotted lines. The arrows represent the action of the map on the boundary of the square: plain arrows represent half edges, and dashed arrows are their images, with matching initial and final symbols. In particular, one sees the expansion of arrows with a circle tail (i.e. the left edge of the square), while the arrows with a square tail (i.e. right side) are expanded only for $\frac{b}{b+1} > \frac{1}{2}$, i.e. $b > 1$.

In the limit $b \to \infty$, $\mu(x; b)$ tends to the constant 1, and the map becomes one dimensional since the first coordinate is fixed in the pair of segments $\{x = \pm 1\}$. In fact, one recognizes the (full) tent map $y \mapsto 1 - 2|y|$, which is known to be chaotic, and in particular conjugate to the full shift on two symbols. Here, the dynamics on the first variable is precisely the coding in question, using $\{\pm 1\}$ as an alphabet. More precisely,

Proposition 2. *In the limit $b, c \to \infty$, the first return map (17) is conjugate to the full tent map T_1. Hence it is chaotic.*

This limit is singular, since the map becomes one-dimensional. Hence, the chaotic behavior of this limit map cannot be used to infer a similar result when one or both parameters b, c are finite. This leads us concentrate on the case when only c is infinite, i.e. map (18) and Figure 7.
Geometrically, this figure is reminiscent of topological horseshoes (see [13]), except that the vertical strips have zero length at their extremities. Because of this degeneracy the whole map is not a topological horseshoe, but by restricting our attention to a suitable subset of the square, for large enough b it is possible to find such a horseshoe. Namely, let us define $I_1 = \mu(I) = [\frac{b}{b+1}, 1]$ and $I_0 = -I_1 = [-1, \frac{-b}{b+1}]$. Let also $J_0 = [0, \frac{b}{b+1}]$, $J_1^- = [-1/2, 0]$ and $J_1^+ = [0, \frac{b}{b+1}]$,

16

and define $A_0 = I_0 \times J_0$, $A_1^\pm = I_1 \times J_1^\pm$, and $A_1 = A_1^- \cup A_1^+$. We also denote $A = A_0 \cup A_1$. Then, one can compute explicitly:

$$F(A_0) = \mathrm{co}\left\{(1,1);\, \mu\left(\tfrac{-b}{b+1}\right)(1,1);\, \mu\left(\tfrac{-b}{b+1}\right)\left(1,\tfrac{1-b}{1+b}\right);\, \left(1,\tfrac{1-b}{1+b}\right)\right\},$$

$$F(A_1^+) = \mathrm{co}\left\{\mu\left(\tfrac{b}{b+1}\right)(1,1);\, \tfrac{b}{b+1}(1,1);\, \tfrac{b}{b+1}\left(1,\tfrac{1-b}{1+b}\right);\, \mu\left(\tfrac{b}{b+1}\right)\left(1,\tfrac{1-b}{1+b}\right)\right\},$$

$$F(A_1^-) = \mathrm{co}\left\{\mu\left(\tfrac{b}{b+1}\right)(-1,1);\, \tfrac{b}{b+1}(-1,1);\, \left(\tfrac{-b}{b+1},0\right);\, \left(-\mu\left(\tfrac{b}{b+1}\right),0\right)\right\},$$

where $\mathrm{co}\{\cdot\}$ denotes the convex hull. The lists above all start with the two upper corners of these image sets, and finish with the lower ones.

In particular, since $\min \mu(I) = \tfrac{b}{b+1}$ one can observe that the upper corners of $F(A_1^-)$ are always above the upper boundary of A_0, and those of both $F(A_1^+)$ and $F(A_0)$ are above the upper boundary of A_1. Also, the lower corners of $F(A_1^-)$ are both exactly on the lower boundary of A_0. Finally, the lower left corner of $F(A_1^+)$ has the highest ordinate among all lower corners of $F(A_0)$ and $F(A_1^+)$, with the value $\tfrac{b(1-b)}{(1+b)^2}$. Thus, these two sets lie entirely across A_1 if the condition $\tfrac{b(1-b)}{(1+b)^2} < -\tfrac{1}{2}$ is fulfilled, i.e. if

$$b > 2 + \sqrt{5} \approx 4.236. \tag{19}$$

Moreover, under this condition the preimages of A_0 and A_1 can be shown to be horizontal strips of the form shown in Figure 8, for instance using the following formula for F^{-1}:

$$F^{-1}(x,y) = \left(\frac{2b}{|x|} - 2b - 1,\ \frac{\mathrm{sgn}(x)}{2}\left(1 - \frac{y}{|x|}\right)\right). \tag{20}$$

One may remark that this inverse map defines a skew-product dynamical system, of the form $(f(x), g(x,y))$, also called a triangular map (see [14]). Thus the dynamics of its first coordinate function provides a lower bound to the complexity of F^{-1}'s dynamics. Remark also that the expression (20) is only defined for $(x,y) \in F(D)$, i.e. for $1 > |x| > \tfrac{b}{b+1}$ and $|y| < |x|$, and in particular it is defined on A.

More generally, iterates of (20) are only defined on the intersection of sets $F^n(D)$, for $n \geq 0$. Furthermore, as usual with horseshoes, a number of points escape A under forward iterations of F; only points lying in the intersection of sets $F^{-n}(A)$, for $n \geq 0$ remain in A. In consequence, one shall consider the dynamics on the invariant set only, defined by

$$A^\infty = \bigcap_{n \in \mathbb{Z}} F^n(A).$$

We will prove that the dynamics on this set has positive entropy, by showing that (A^∞, F) conjugates with the golden mean shift (Σ', σ), defined as the space of bi-infinite sequences

$$\Sigma' = \{\ldots s_{-2} s_{-1}.s_0 s_1 s_2 \ldots : s_i \in \{0,1\},\ s_i s_{i+1} \neq 00,\ i \in \mathbb{Z}\}, \tag{21}$$

endowed with the product topology, e.g. given by the metric

$$d((s_n),(t_n)) = 2^{-\inf\{|k| : s_k \neq t_k\}}, \quad \text{with} \quad 2^{-\infty} = 0. \tag{22}$$
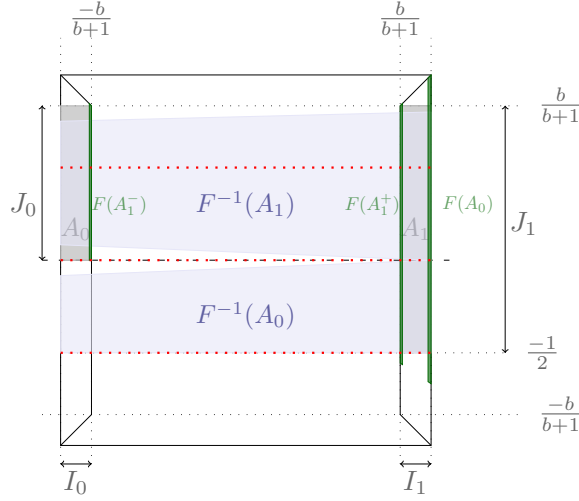
Figure 8: The two sets A_0, A_1, their images and pre-images, for $b = 5$ (hence $b > 2 + \sqrt{5}$).

This metric is of course defined on the whole set $\Sigma = \{0,1\}^{\mathbb{Z}}$, as well as on $\Sigma_+ = \{0,1\}^{\mathbb{N}}$. The map $\sigma : \Sigma' \to \Sigma'$ is the shift map $\sigma(...s_{-2}s_{-1}.s_0s_1...) = ...s_{-1}s_0.s_1s_2...$

Let us first consider only the set of points whose backward iterates are all in A, namely

$$A^{+\infty} = \bigcap_{n \geq 0} F^n(A). \tag{23}$$

Since A is compact, note that $A^{+\infty}$ is the ω-limit set of the map F. From the expression of F in (18) it follows that each vertical line of the form $\{x\} \times I$ is mapped to a pair of intervals included in the vertical lines $\{\pm\mu(x)\} \times I$. Moreover, the preceding discussion shows that provided $b > 2 + \sqrt{5}$, if one considers the restriction of the dynamics to A, any vertical interval $\{x\} \times J_0$ across A_0 will be sent to $\{\mu(x)\} \times J_1$, whereas a line $\{x\} \times J_1$ across A_1 will be sent to the pair of intervals $\{-\mu(x)\} \times J_0 \cup \{\mu(x)\} \times J_1$. It is thus sufficient to consider the one dimensional dynamics obtained by projection on abscissas to characterize entirely the set $A^{+\infty}$.

To do so we first consider, without restriction to the set A, iterations of the projection F_1. For any x, the image $F_1(\{x\} \times I)$ is two-valued, with branches shown here for $b = 1.5$:
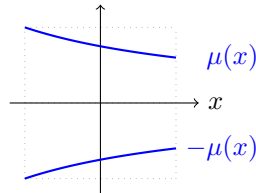
However, we have observed in (20) that the first coordinate of the inverse map F^{-1} is a real-valued map, which will be more convenient. We denote it $v : I \to I$

for the sake of the current discussion; it is shown here for $b = 1.5$:

$$v(x) = \mu^{-1}(|x|)$$
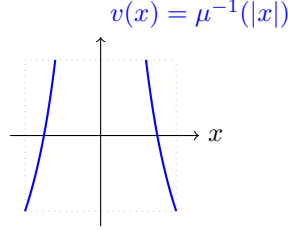
One sees that the central interval $I \setminus (I_0 \cup I_1)$ escapes the domain I under v, and more generally the set of points which remain in I under all forward iterations of v is a Cantor set. By construction it is also exactly the set of x values that can be reached under forward iterations of F_1, but its components are more easily described in terms of v, as limits of the following:

$$I_{s_0...s_n} = \bigcap_{i=0}^{n} v^{-i}(I_{s_i}), \qquad \text{for} \quad n \in \mathbb{N},\ (s_0, ..., s_n) \in \{0,1\}^n.$$

By continuity of v on the compact intervals I_0 and I_1 and the fact that $v(I_0) = v(I_1) = I$, it follows that all $I_{s_0...s_n}$ are nonempty compact intervals. Let now $s = (s_i) \in \Sigma_+$. Then, for all $n \geq 0$ one has $I_{s_0...s_n} \supset I_{s_0...s_n, s_{n+1}}$, and thus

$$I_s = \bigcap_{n \geq 0} I_{s_0...s_n}$$

is a nonempty compact set, a limit of nested nonempty compact sets. Now, from (20) one deduces that the absolute value of the slope of v on I is bounded below by its value at ± 1, which is $2b$. It follows that $|v(x_1) - v(x_2)| \geq 2b|x_1 - x_2|$ if x_1, x_2 are both in I_0 or I_1. Therefore, if $s_0 s_1 ... s_n$, $s_i \in \{0,1\}$ is any list and $v^i(x_1), v^i(x_2) \in I_{s_i}$ then $|v^n(x_1) - v^n(x_2)| \geq (2b)^n|x_1 - x_2|$. Hence for $b > \frac{1}{2}$, and *a fortiori* when (19) holds, the length of intervals I_s is zero for $s \in \Sigma_+$, and being nonempty they are singletons. Note here that the I_s are the components of the Cantor set mentioned earlier, which can thus be denoted as

$$\Lambda = \bigcup_{s \in \Sigma_+} I_s.$$

In other words, for any $s \in \Sigma_+$, there exists one and only one point $X(s)$ in Λ such that $I_s = \{X(s)\}$. Furthermore, with the metric d defined in (22) it is a standard exercise to show that the map X thus defined is not only bijective, but in fact a homeomorphism $\Sigma_+ \to \Lambda$ (see e.g. [22]).

To this point, we have only considered the abscissas of points in D under forward iterations, and seen that they form the Cantor set Λ. It follows that $F^{+\infty} = \bigcap_{n \geq 0} F^n(D) \subset \Lambda \times I$. This inclusion is strict both because some vertical components are strict subsets of I, and because it may happen that the vertical components of the form $F_2^n(\{x\} \times I)$ vanish in the limit $n \to +\infty$ of infinite iterations, in which case x does not even belong to the first projection of $F^{+\infty}$. In fact, it is clear that the first projection of $F^{+\infty}$ is exactly the subset of Λ where this phenomenon does not happen. But we have seen earlier that on the

subdomain A, the vertical component of forward iterates does not shrink, and is always J_0 on A_0 and J_1 on A_1, with the only constraint that points in A_0 are always mapped on A_1. In other words, the vertical component of $A^{+\infty}$ is the same as A, and the horizontal component is $\Lambda' = \bigcup_{s \in \Sigma'_+} I_s$, where $\Sigma'_+ \subset \Sigma_+$ is the restriction of the golden mean shift space (21) to nonnegative indices. In other words,

$$A^{+\infty} = \bigcup_{s=(s_i) \in \Sigma'_+} I_s \times J_{s_0}. \tag{24}$$

To include the backward dynamics, we have to consider the intersection of the set $A^{+\infty}$ above with the backwards limit set $A^{-\infty} = \bigcap_{n \geq 0} F^{-n}(A)$. Now, it can be intuited from Figure 8 that this amounts to restricting the vertical component only, since $F^{-1}(A_i)$ extends over the whole square D in the horizontal direction, for both $i \in \{0, 1\}$. In fact, the situation is similar to the preceding discussion, reversing the roles of horizontal and vertical directions. The vertices of pre-images of A_0 and A_1 can be computed explicitly, as were their direct images:

$$F^{-1}(A_0) = \mathrm{co} \left\{ \left(-1, -\tfrac{1}{2}\right); \left(1, -\tfrac{1}{2}\right); (1, 0); \left(-1, \tfrac{-1}{2(b+1)}\right) \right\},$$

$$F^{-1}(A_1) = \mathrm{co} \left\{ \left(-1, \tfrac{1}{2(b+1)}\right); (1, 0); \left(1, \tfrac{3}{4} + \tfrac{1}{4b}\right); \left(-1, \tfrac{3}{4}\right) \right\}.$$

It appears that both sets above intersect A_1, and $F^{-1}(A_1)$ furthermore intersects A_0 (but not $F^{-1}(A_0)$). On the x axis, these non-empty intersections in fact cover I_0 and I_1, and the vertical components are included in J_0 and J_1 respectively, provided the upper-right vertex of $F^{-1}(A_1)$ is below the upper-right vertex of A_1. This condition reads $\tfrac{3}{4} + \tfrac{1}{4b} < \tfrac{b}{b+1}$, which is equivalent to $b > 2 + \sqrt{5}$, the same condition (19) we have seen for the forward iterates. In other words, under this condition the sets $F^{-1}(A_{s_{-1}}) \cap A_{s_0}$ are nonempty for $(s_0, s_{-1}) \neq (0, 0)$, and of the form $I_{s_0} \times J_{s_0 s_{-1}}$, with $J_{s_0 s_{-1}}$ a compact sub-interval of J_{s_0}. As before, we can thus define by induction nonempty compact intervals $J_{s_0 \ldots s_{-n}}$ as the vertical components of $\bigcap_{0 \geq k \geq -n} F^k(A_{s_k})$, provided all pairs (s_k, s_{k-1}) differ from $(0, 0)$. Being compact, these intervals allow us to define non empty compact sets $J_s = \bigcap_{n \leq 0} J_{s_0 \ldots s_n}$ for all infinite sequences $s \in \Sigma'_-$, the one-sided golden mean shift with nonpositive indices. Finally, one can prove that these nonempty compact sets are in fact singletons as follows; from (20) one deduces that the partial derivative $\frac{\partial F_2^{-1}}{\partial y}$ of the vertical coordinate of F^{-1} has a modulus $\frac{1}{2|x|}$, and this coordinate function is thus contracting for all $|x| > \tfrac{1}{2}$. Since $|x| > \frac{b}{b+1}$ on A, this holds for $b > 1$, and thus in particular under the condition (19). Hence, for any $s \in \Sigma'_-$, one has $\bigcap_{k \leq 0} F^k(A_{s_k}) = I_{s_0} \times J_s$, where J_s is a singleton, and

$$A^{-\infty} = \bigcup_{s=(s_i) \in \Sigma'_-} I_{s_0} \times J_s.$$

Since forward (resp. backward) iterates do not affect the vertical (resp. horizontal) component of A, we may extend the definition of the singletons I_s, J_s to bi-infinite subscripts, by letting $I_s = I_{s_0 s_1 s_2 \ldots}$ (resp. $J_s = J_{\ldots s_{-2} s_{-1} s_0}$) for any sequence $s = (\ldots s_{-1} s_0 s_1 \ldots) \in \Sigma'$, the golden mean shift (21). Then, the

previous discussion implies

$$A^\infty = \bigcup_{s=(s_i)\in\Sigma'} I_s \times J_s,$$

where each product $I_s \times J_s$ above is a single point in A. This defines a bijection $S : A^\infty \to \Sigma'$, which can easily be proven to be a homeomorphism, with the metric (22). Moreover, it is readily verified that $S \circ F(x, y) = \sigma \circ S(x, y)$ for any $(x, y) \in A^\infty$. In summary we have proven the following.

Proposition 3. *Assume that b satisfies inequality* (19). *Then, the map S is a conjugacy between the dynamical systems (A^∞, F) and (Σ', σ).*

In particular, these two systems have identical topological entropy, which implies $h(F|_{A^\infty}) > 0$.

An important remark at this point is that the whole preceding discussion is essentially topological: the corners of A_0, A_1 or their images can be moved slightly in Figure 8 without affecting the rest of the discussion. In particular, it can be verified that $A^{-\infty}$ is at a positive distance from the discontinuity line $I \times \{0\}$. Hence one may remove a small positive band of the form $I \times (-\varepsilon, \varepsilon)$ around the discontinuity line from the set A without affecting A^∞, justifying *a posteriori* or choice of considering the extensions of F to this line.

In other words, the invariant set A^∞ is structurally stable, which allows us to return to our original system by perturbation arguments, as we discuss now.

5.4. The case c finite

In the case where both b and c are finite, the first return map (18) also depends on the parameter c. Denoting $\epsilon = \frac{1}{c}$ to be able to deal with a limit $\epsilon \to 0$, the maps (16) can be rewritten as a function depending on the parameters b and ϵ. From the generic form in Equation (16) and the expressions of maps at boxes 101, 111 and 121, it appears that both b and ϵ appear in fractional linear terms in the local map expressions, and that they are never poles of these. From these expressions, one deduces that the full return map depend on both b and ϵ through rational functions, of order one in b (which only occur in the map at box 101), and of higher order in ϵ. The latter is moreover not a pole of these rational functions, since it always occur in terms of the form $\theta_i + \frac{1}{\epsilon} - x_i$ with $x_i < \theta_i$, or $\theta_i - \frac{1}{\epsilon} - x_i$ with $x_i > \theta_i$. This claim is further confirmed by explicit computation of this return map, as shown in the Appendix.

These rational function terms imply that the dependence of the return map on the parameter ϵ is smooth (in fact, C^∞). At $\epsilon = 0$, the map (18) is found exactly, and for ϵ small enough the corner points of $F(A_0)$ and $F^\pm(A_1)$ can be chosen arbitrarily close to their limit value (for $\epsilon \to 0$). Since the vertical bands of the form $F(A_i) \cap A_j$ are either empty (for $(i, j) = (0, 0)$) or have positive width, there is an open neighborhood of $\epsilon = 0$ for which the nonempty ones will still have positive width. Similarly, the horizontal bands $F^{-1}(A_i) \cap A_j$ have a positive height for an nonempty interval of ϵ values. Finally, from the C^1 dependency on ϵ one deduces that the contraction and expansion rates of F in the horizontal and vertical directions remain away from the value 1 for small ϵ. In other words, for such ϵ the regions A_0 and A_1 will still respect all the conditions which ensure conjugacy with the golden mean shift:

Proposition 4. *There exists an open interval of positive values for the parameter ϵ for which the map $F(x, y; \epsilon)$ remains conjugate to the golden-mean shift.*

Finally, we have performed numerical simulations, to illustrate our results at least visually. In Figures 9 and 10, we show example trajectories for particular values of b and c. Very similar trajectories have been observed for any other values, provided they were both large enough.
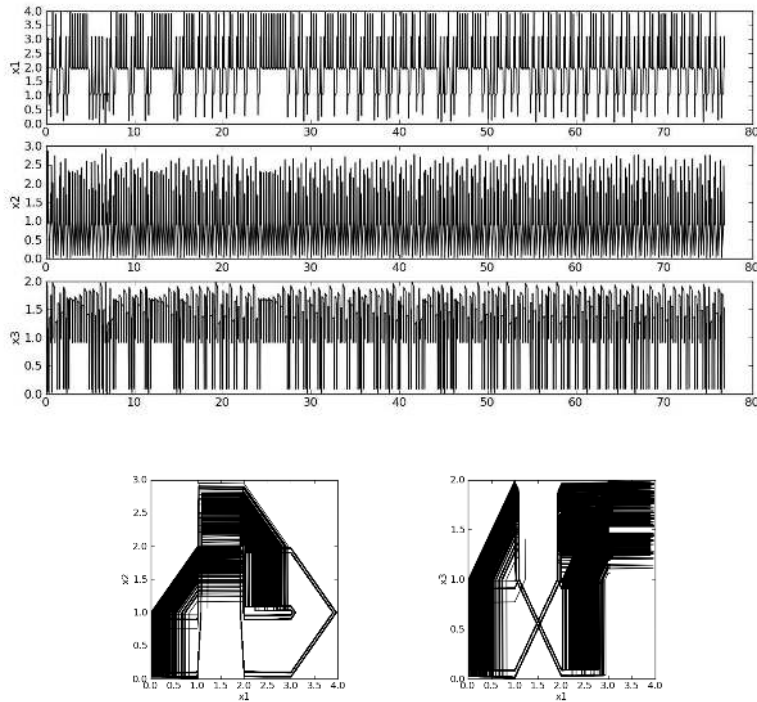

Figure 9: Orbit of a randomly chosen point on the wall W, for $b = 5$, $c = 50$, after 5000 wall intersections. The three coordinates vs. time are shown above, and 2-dimensional projections below.

6. Embedding result

In general, our system (1) has $\kappa(x)$ depending on $x \in \mathbb{R}^n$ only through step functions of the components, x_i. Thus, the system takes the form

$$\frac{dx_i}{dt} = -\gamma_i x_i + f_i \left(s^+(x_1, \theta_1^1), s^+(x_1, \theta_1^2), \ldots, s^+(x_n, \theta_n^{q_n-1}) \right) \qquad (25)$$

for $i = 1, \ldots, n$, where s^- terms are included as $1 - s^+$ and f_i is a function of its binary vector argument, which can take on only a finite number of values.

Now define

$$y_{im} = x_i - \theta_i^m, \quad i = 1, \ldots, n, \quad m = 1, \ldots, q_i - 1. \qquad (26)$$
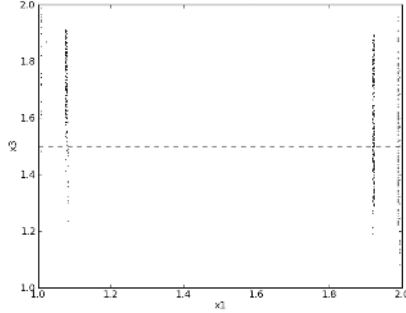
Figure 10: Poincaré section of the orbit shown in Figure 9. The dashed line represents the separatrix between the two cycles.

Note that each $q_i \geq 2$, since each variable has at least one non-trivial threshold, aside from $\theta_i^0 = 0$ and $\theta_i^{q_i}$, a maximum value for x_i. Thus, the system (26) has $N = \sum_{i=1}^{n}(q_i - 1)$ equations, where $N \geq n$, and $y = (y_{11}, \ldots, y_{n,(q_n-1)})$ can be considered as a vector in $\mathbb{R}^N$.

With this definition, we can write

$$
\begin{aligned}
s^+(x_i, \theta_i^m) &= s^+(y_{im}, 0) = Y_{im} \\
s^-(x_i, \theta_i^m) &= s^-(y_{im}, 0) = 1 - Y_{im} = \bar{Y}^{im}
\end{aligned}
$$

where Y and $\bar{Y}$ are defined by the second equality in the first line above. Using these new definitions, we can write the system (25) as a system in $\mathbb{R}^N$:

$$
\begin{aligned}
\frac{dy_{im}}{dt} &= -\gamma_i(y_{im} + \theta_i^m) + f_i\left(Y_{11}, Y_{12}, \ldots, Y_{n,(q_n-1)}\right) \quad (27) \\
&= -\gamma_i y_{im} + g_{im}\left(Y_{11}, Y_{12}, \ldots, Y_{n,(q_n-1)}\right). \quad (28)
\end{aligned}
$$

Of course, for this system in $\mathbb{R}^N$ to be equivalent to the original system in $\mathbb{R}^n$, it must be restricted to an n-dimensional subspace, and this is given via the embedding equations (26) by imposing

$$
y_{ik} - y_{i\ell} = \theta_i^\ell - \theta_i^k, \quad i = 1, \ldots, n, \quad k \neq \ell \in \{1, \ldots, q_i - 1\}.
$$

However, if we consider (27) in all of $\mathbb{R}^N$ without restriction, we note that

$$
\frac{d}{dt}(y_{ik} - y_{i\ell}) = -\gamma_i\left[(y_{ik} - y_{i\ell}) - (\theta_i^\ell - \theta_i^k)\right].
$$

Thus, the subspace of $\mathbb{R}^N$ defined by setting all $y_{ik} - y_{i\ell} = \theta_i^\ell - \theta_i^k$ is invariant and corresponds to the original system in $\mathbb{R}^n$. Moreover, all trajectories everywhere in $\mathbb{R}^N$ converge exponentially to this subspace, so the asymptotic behaviour of (27) in $\mathbb{R}^N$ is identical to that of (25) in $\mathbb{R}^n$.

The implication of this embedding for the purpose of the current study is that any behaviour that is possible in multi-threshold gene networks (chaos, for example) is also possible in single-threshold gene networks, though the cost is an increase in dimension. In fact, the implications are much broader. All the

23

theory that is developed for single-threshold networks in their full generality (not restricted to classes that preclude the invariant subspace implied by the embedding, for example) can be brought to bear on multi-threshold networks as well.

The example of Section 5 can be rendered as a 6-dimensional system with a single threshold per variable, by following the above embedding procedure. One possible set of differential equations corresponding to the example described in Section 5 is as follows:

$$
\begin{aligned}
\frac{dx_1}{dt} &= -x_1 + \left[\frac{1}{2} + s^+(x_1, \theta_{11}) + s^+(x_1, \theta_{12}) + s^+(x_1, \theta_{13})\right] \\
&\quad + \left(\frac{1}{2} + c\right)\left[s^+(x_3, \theta_{31})(1 - s^-(x_2, \theta_{21})[s^+(x_1, \theta_{11}) - s^+(x_1, \theta_{12})]) - s^+(x_2, \theta_{21})\right. \\
&\quad + s^+(x_1, \theta_{12})(3s^+(x_2, \theta_{21}) + s^+(x_2, \theta_{22}) - 2) \\
&\quad \left. + 2(s^+(x_1, \theta_{11}) - s^+(x_1, \theta_{12}))s^+(x_2, \theta_{22})s^-(x_3, \theta_{31})\right] \\
\frac{dx_2}{dt} &= -x_2 + \left[\frac{1}{2} + s^+(x_2, \theta_{21}) + s^+(x_2, \theta_{22})\right] \\
&\quad + \left(\frac{1}{2} + c\right)\left[s^+(x_1, \theta_{11}) - s^+(x_1, \theta_{12}) - s^+(x_1, \theta_{13}) + s^+(x_3, \theta_{31}) - 1\right] \\
&\quad + (b - c)\left[(s^+(x_1, \theta_{11}) - s^+(x_1, \theta_{12}))s^-(x_2, \theta_{21})s^+(x_3, \theta_{31})\right] \\
\frac{dx_3}{dt} &= -x_3 + \left[\frac{1}{2} + s^+(x_3, \theta_{31})\right] \\
&\quad + \left(\frac{1}{2} + c\right)\left[s^-(x_1, \theta_{11})s^-(x_2, \theta_{21}) + (s^+(x_1, \theta_{12}) - s^+(x_1, \theta_{13}))(s^+(x_2, \theta_{21}) - s^+(x_2, \theta_{22}))\right. \\
&\quad \left. - (s^+(x_1, \theta_{11}) - s^+(x_1, \theta_{12}))s^+(x_2, \theta_{21})\right] \\
&\quad + \left(\frac{1}{2}c\right)\left[s^-(x_1, \theta_{12})s^+(x_2, \theta_{21})s^+(x_3, \theta_{31})\right]
\end{aligned}
$$

The corresponding system embedded in $\mathbb{R}^6$ is then:

$$\frac{dy_1}{dt} = -y_1 - 1 + \frac{1}{2} + Y_1 + Y_2 + Y_3$$
$$+ \left(\frac{1}{2} + c\right)[Y_6(1 - \bar{Y}_4(Y_1 - Y_2) - Y_4 + Y_2(3Y_4 + Y_5 - 2) + 2(Y_1 - Y_2)Y_5\bar{Y}_6]$$

$$\frac{dy_2}{dt} = -y_2 - 2 + \frac{1}{2} + Y_1 + Y_2 + Y_3$$
$$+ \left(\frac{1}{2} + c\right)[Y_6(1 - \bar{Y}_4(Y_1 - Y_2) - Y_4 + Y_2(3Y_4 + Y_5 - 2) + 2(Y_1 - Y_2)Y_5\bar{Y}_6]$$

$$\frac{dy_3}{dt} = -y_3 - 3 + \frac{1}{2} + Y_1 + Y_2 + Y_3$$
$$+ \left(\frac{1}{2} + c\right)[Y_6(1 - \bar{Y}_4(Y_1 - Y_2) - Y_4 + Y_2(3Y_4 + Y_5 - 2) + 2(Y_1 - Y_2)Y_5\bar{Y}_6]$$

$$\frac{dy_4}{dt} = -y_4 - 1 + \frac{1}{2} + Y_4 + Y_5 + \left(\frac{1}{2} + c\right)[Y_1 - Y_2 - Y_3 + Y_6 - 1] + (b - c)[(Y_1 - Y_2)\bar{Y}_4 Y_6]$$

$$\frac{dy_5}{dt} = -y_5 - 2 + \frac{1}{2} + Y_4 + Y_5 + \left(\frac{1}{2} + c\right)[Y_1 - Y_2 - Y_3 + Y_6 - 1] + (b - c)[(Y_1 - Y_2)\bar{Y}_4 Y_6]$$

$$\frac{dy_6}{dt} = -y_6 - 1 + \frac{1}{2} + Y_6 + \left(\frac{1}{2} + c\right)[\bar{Y}_1\bar{Y}_4 + (Y_2 - Y_3)(Y_4 - Y_5) - (Y_1 - Y_2)Y_4] + \left(\frac{1}{2}c\right)[\bar{Y}_2 Y_4 Y_6]$$

where

$$
\begin{aligned}
y_1 &= x_1 - 1, & Y_1 &= s^+(x_1, 1) \\
y_2 &= x_1 - 2, & Y_2 &= s^+(x_1, 2) \\
y_3 &= x_1 - 3, & Y_3 &= s^+(x_1, 3) \\
y_4 &= x_2 - 1, & Y_4 &= s^+(x_2, 1) \\
y_5 &= x_2 - 2, & Y_5 &= s^+(x_2, 2) \\
y_6 &= x_3 - 1, & Y_6 &= s^+(x_3, 1)
\end{aligned}
$$

The boundary between boxes 101 and 111, which serves as a Poincaré section in the example of Section 5 becomes, in the larger space, the boundary between the $+ - - - -+$ orthant and the $+ - - + -+$ orthant, where y_4 switches from negative to positive, which means that on the invariant subspace corresponding to the original system, x_2 switches across $\theta_{21} = 1$.

7. Discussion

The study of Glass networks has led a number of authors to describe chaotic dynamics in example systems. Most often, the latter have been obtained after scanning families of randomly generated examples. Here, we have proposed a method to explicitly construct examples of complex behaviour in Glass networks. This method is based on a geometric point of view, where the transition maps between walls are first considered in the limit where focal points are infinitely remote, which corresponds to a limit in which degradation rates go to zero. The finite case is then obtained by relying on the structural stability of

the limit case.

We have illustrated our method with an example in $\mathbb{R}^3$, in which several thresholds per variable are used. As an auxiliary result, we have shown that any system with several thresholds can be embedded in a binary Glass network.

Acknowledgement

Appendix A. Expression of the return map for $b, c < \infty$

Though lengthy, we provide here the expression of the return map of our example for finite b and c, rescaled to be a map of the square $[-1, 1]^2$. All computations were performed using the software sage[1] and the corresponding files are available upon request.

We introduce the notation $\epsilon = \frac{1}{c}$. Then the limit of the expressions below as $\epsilon \to 0$ gives exactly the map (18). The return map decomposes in two maps: $F^-(x, y; \epsilon)$ is the return map through the short cycle, i.e. for $y < 0$, and $F^+(x, y; \epsilon)$ the map through the long cycle, i.e. $y > 0$. Both these maps have coordinate functions which write as rational functions of the parameter ϵ. For sake of readability, we present the numerators and denominators of separately, denoting them $\mathrm{num}F_i^{\pm}$ and $\mathrm{den}F_i^{\pm}$, respectively. With such conventions, we get:

$$
\begin{aligned}
\mathrm{num}F_1^- \;=\; & (by + b)\epsilon^5 - 2\,(bx + 14\,by + 15\,b)\epsilon^4 \\
& -4\,(5\,bx + 24\,by + 29\,b)\epsilon^3 - 8\,(5\,bx + 18\,by + 23\,b)\epsilon^2 \\
& -32\,(bx + 3\,by + 4\,b)\epsilon - 32\,b
\end{aligned}
$$

$$
\begin{aligned}
\mathrm{den}F_1^- \;=\; & ((2\,b + 1)y + 2\,b + 1)\epsilon^5 + ((2\,b + 1)x + 4\,(7\,b + 4)y + 30\,b + 17)\epsilon^4 \\
& +4\,(8\,(3\,b + 2)y + (5\,b + 3)x + 29\,b + 19)\epsilon^3 \\
& +4\,(12\,(3\,b + 2)y + (10\,b + 7)x + 46\,b + 31)\epsilon^2 \\
& +16\,(2\,(b + 1)x + 3\,(2\,b + 1)y + 8\,b + 5)\epsilon + 32\,b + 16\,x + 16
\end{aligned}
$$

$$
\begin{aligned}
\mathrm{num}F_2^- \;=\; & (by + b)\epsilon^5 + 2\,(bx + 12\,by + 13\,b)\epsilon^4 + 16\,(bx + 4\,by + 5\,b)\epsilon^3 \\
& +24\,(bx + 4\,by + 5\,b)\epsilon^2 + 96\,(by + b)\epsilon + 64\,by + 32\,b
\end{aligned}
$$

$$
\begin{aligned}
\mathrm{den}F_2^- \;=\; & ((2\,b + 1)y + 2\,b + 1)\epsilon^5 + ((2\,b + 1)x + 4\,(7\,b + 4)y + 30\,b + 17)\epsilon^4 \\
& +4\,(8\,(3\,b + 2)y + (5\,b + 3)x + 29\,b + 19)\epsilon^3 \\
& +4\,(12\,(3\,b + 2)y + (10\,b + 7)x + 46\,b + 31)\epsilon^2 \\
& +16\,(2\,(b + 1)x + 3\,(2\,b + 1)y + 8\,b + 5)\epsilon + 32\,b + 16\,x + 16
\end{aligned}
$$

---

[1] http://www.sagemath.org

$$\text{num}F_1^+ = 2\,(by+b)\epsilon^8 - 2\,(bx-7\,by-4\,b)\epsilon^7 - 2\,(3\,bx-4\,by-7\,b)\epsilon^6$$
$$-4\,(2\,bx+19\,by+7\,b)\epsilon^5 + 4\,(17\,bx-58\,by-47\,b)\epsilon^4$$
$$+8\,(23\,bx-48\,by-57\,b)\epsilon^3 + 16\,(7\,bx-18\,by-35\,b)\epsilon^2$$
$$-64\,(by+5\,b)\epsilon - 64\,b$$

$$\text{den}F_1^+ = ((2\,b+1)y+2\,b+1)\epsilon^8 - ((2\,b+1)x-2\,(7\,b+4)y-8\,b-5)\epsilon^7$$
$$-2\,((3\,b+2)x-(4\,b+7)y-7\,b-7)\epsilon^6$$
$$-2\,((4\,b+5)x+(38\,b+3)y+14\,b-6)\epsilon^5$$
$$-2\,(4\,(29\,b+8)y-(34\,b+7)x+94\,b+15)\epsilon^4$$
$$+8\,((23\,b+8)x-2\,(24\,b+7)y-57\,b-15)\epsilon^3$$
$$+8\,(7\,(2\,b+1)x-4\,(9\,b+2)y-70\,b-19)\epsilon^2$$
$$-32\,((2\,b+1)y+10\,b+3)\epsilon - 64\,b-32\,x-32$$

$$\text{num}F_2^+ = -4\,(by+b)\epsilon^5 + 4\,(bx-8\,by-5\,b)\epsilon^4$$
$$+16\,(bx-2\,by-2\,b)\epsilon^3 + 16\,(bx+4\,by-5\,b)\epsilon^2$$
$$+64\,(3\,by-2\,b)\epsilon + 128\,by - 64\,b$$

$$\text{den}F_2^+ = ((2\,b+1)y+2\,b+1)\epsilon^8 - ((2\,b+1)x-2\,(7\,b+4)y-8\,b-5)\epsilon^7$$
$$-2\,((3\,b+2)x-(4\,b+7)y-7\,b-7)\epsilon^6$$
$$-2\,((4\,b+5)x+(38\,b+3)y+14\,b-6)\epsilon^5$$
$$-2\,(4\,(29\,b+8)y-(34\,b+7)x+94\,b+15)\epsilon^4$$
$$+8\,((23\,b+8)x-2\,(24\,b+7)y-57\,b-15)\epsilon^3$$
$$+8\,(7\,(2\,b+1)x-4\,(9\,b+2)y-70\,b-19)\epsilon^2$$
$$-32\,((2\,b+1)y+10\,b+3)\epsilon - 64\,b-32\,x-32$$

[1] R. Casey, H. de Jong, J.L. Gouzé, *Piecewise-linear Models of Genetic Regulatory Networks: Equilibria and their Stability*, J. Math. Biol., 52(1):27-56 (2006).

[2] P. Collet, J.-P. Eckmann, *Iterated maps of the interval as dynamical systems*, Birkhäuser 1980.

[3] H. de Jong, *Modeling and simulation of genetic regulatory systems : a literature review*, Journal of Computational Biology 9(1):67-103 (2002).

[4] H. de Jong, J.L. Gouzé, C. Hernandez, M. Page, T. Sari, J. Geiselmann, *Qualitative simulation of genetic regulatory networks using piecewise-linear models*, Bulletin of Mathematical Biology, 66(2):301-340 (2004).

[5] R. Edwards, *Analysis of continuous-time switching networks*, Physica D 146:165-199 (2000).

[6] R. Edwards, *Chaos in neural and gene networks with hard switching*, Differential Equations and Dynamical Systems, 9:187-220 (2001).

[7] E. Farcot, *Geometric properties of piecewise affine biological network models*, J. Math. Biol, 52(3):373-418 (2006).

[8] E. Farcot, *Symbolic numeric analysis of attractors in randomly generated piecewise affine models of gene networks*, ISSAC 2006 proceedings, pp. 79–86 (2006).

[9] T. Gedeon, *Attractors in continuous time switching networks*, Communications on Pure and Applied Analysis (CPAA) vol. 2, No. 2, 187-209, (2003).

[10] L. Glass, *Combinatorial and topological methods in nonlinear chemical kinetics*, J. Chem. Phys. 63:1325-1335 (1975).

[11] J.L. Gouzé, T. Sari, *A class of piecewise linear differential equations arising in biological models*, Dynamical systems, 17:299–316 (2003).

[12] J. Guckenheimer, P. Holmes, *Nonlinear Oscillations, Dynamical Systems, and Bifurcations of Vector Fields*, Springer Verlag 1983.

[13] J. Kennedy, J.A. Yorke, *Topological Horseshoes*, Transactions of the American Mathematical Society, 353(6):2513–2530 (2001).

[14] S. F. Kolyada, *On dynamics of triangular maps of the square*, Erg. Theory and Dyn. Sys., 12(4):749–768 (1992).

[15] Q. Li, X.-S. Yang, *Chaotic dynamics in a class of three dimensional Glass networks*, Chaos 16, 033101 (2006).

[16] T. Mestl, E. Plahte, S.W. Omholt, *Periodic solutions of piecewise-linear differential equations*, Dyn. Stab. Syst. 10(2):179-193 (1995).

[17] T. Mestl, C. Lemay, L. Glass, *Chaos in high-dimensional neural and gene networks*, Physica D, 98:33-52 (1996).

[18] M. Misiurewicz, P. Raith, *Strict inequalities for the entropy of transitive piecewise monotone maps*, Discrete Contin. Dynam. Sys. 13:451–468 (2005).

[19] M. Misiurewicz, P. Zgliczynski, *Topological entropy for multidimensional perturbations of one-dimensional maps*, Internat. J. Bifur. Chaos, 11:1443–1446 (2001).

[20] E. Plahte, T. Mestl, S.W. Omholt, *A methodological basis for description and analysis of systems with complex switch-like interactions*, J. Math. Bio. 36:321-348 (1998).

[21] E. Plahte, S. Kjøglum, *Analysis and generic properties of gene regulatory networks with graded response functions*, Physica D, 201:150-176 (2005).

[22] C. Robinson, *Dynamical Systems: Stability, Symbolic Dynamics and Chaos*, CRC Press, Florida, 1999.

[23] S. Smale, *Differentiable dynamical systems*, Bull. Amer. Math. Soc. 73:747-817 (1967).